

Phonon amplification in two coupled cavities containing one mechanical resonator

Hui Wang,^{1,2} Zhixin Wang,² Jing Zhang,^{3,4} Şahin Kaya Özdemir,⁵ Lan Yang,⁵ and Yu-xi Liu^{1,2,4,*}

¹*Institute of Microelectronics, Tsinghua University, Beijing 100084, China*

²*Department of Microelectronics and Nanoelectronics, Tsinghua University, Beijing 100084, China*

³*Department of Automation, Tsinghua University, Beijing 100084, P. R. China*

⁴*Tsinghua National Laboratory for Information Science and Technology (TNList), Beijing 100084, China*

⁵*Department of Electrical and Systems Engineering, Washington University, St. Louis, MO 63130, USA*

(Dated: February 29, 2024)

We study a general theory of phonon lasing [I. S. Grudinin *et al.*, Phys. Rev. Lett. **104**, 083901 (2010)] in coupled optomechanical systems. We derive the dynamical equation of the phonon lasing using supermodes formed by two cavity modes. A general threshold condition for phonon lasing is obtained. We also show the differences between phonon lasing and photon lasing, generated by photonic supermodes and two-level atomic systems, respectively. We find that the phonon lasing can be realized in certain parameter regime near the threshold. The phase diagram and second-order correlation function of the phonon lasing are also studied to show some interesting phenomena that cannot be observed in the common photon lasing with the two-level systems.

PACS numbers: 42.50.Dv, 03.67.Mn, 42.50.Ct, 74.50.+r

I. INTRODUCTION

Phonons are quanta of sound and are very important concept in condensed matter physics. They exist as vibrating modes in various physical systems, including single trapped ions [1], atoms in solid-state materials [2], and macroscopic mechanical resonator [3]. Phonons are very similar to photons in the sense that both are bosonic particles and obey Bose-Einstein statistics. Thus, the phenomena occurred in photons are quite often brought to phonons. For instance, in analogue to coherent and squeezed photon states, squeezed phonon states [4] have been proposed to be generated in bulk solid-state materials by using second-order Raman scattering and explored to modulate quantum fluctuations of atomic displacements. The coherent phonon generation via impulsive stimulated Raman scattering in the condensed media [5] and the phonon stimulated emission have also been studied [6–9].

Reaching the quantum mechanical regime for vibrating modes of macroscopic mechanical resonators is a longstanding goal [3]. Both mechanical resonators and single-mode cavity fields can be modeled as harmonic oscillators. Thus, it is reasonable to expect that mechanical resonators can play the role of single-mode cavities in quantum optics, and help to realize mechanical quantum electrodynamics (QED) by replacing the single-mode cavity field with a mechanical resonator in its quantum regime. Experimentalists have showed that the usual Jaynes-Cumming model in the cavity QED can be realized by coupling a superconducting qubit to a mechanical resonator [10–12]. Also several methods have been developed in optomechanical systems for cooling the mechanical resonators with low frequencies to their quantum ground states by coupling them to single-mode microwave or optical fields via the radiation pressure [13]. These achievements lay a solid foundation to develop single-mode phonon

cavity [14] and manipulate phonon states [15, 16] at single-photon level [17, 18] using mechanical resonators.

It well known that lasing can be generated when the stimulated emission is coherently amplified by a gain medium inside a cavity. Similar to the lasing, several theoretical proposals were put forward to generate phonon coherent amplification of stimulated emission in different systems, e.g., the quantum dot [19], ultra-cold atomic gas [20], nanomagnets [21], acoustical cavities [22], and double barrier systems [23]. The amplification of mechanical oscillations was also theoretically studied by coupling a nanomechanical resonator to polarized paramagnetic nuclei [24]. Such so-called phonon lasing was experimentally demonstrated in the systems of vibrating microscopic particles (e.g., trapped magnesium ions [25]), electromechanical resonator [26], and superlattice structures [27]. Recently reported several experiments on phonon lasing in optomechanical systems [28, 29] and also in an optomechanical system coupled to a cavity [30] are of particular interest, and have been focus of attention.

In the experiment reported in Ref. [30], two degenerate microtoroid whispering gallery mode (WGM) optical resonators are coupled in a controllable way through the evanescent fields, and one of them is coupled to a mechanical resonator via radiation pressure. These two coupled optical cavities form two supermodes acting as a controllable two-level system which can be tuned to resonantly interact with the mechanical resonator. This ingenious design is very similar to the laser system with two-level atoms interacting with single-mode cavity fields [31]. Although the threshold condition on phonon lasing in the coupled cavity system has been discussed in Ref. [30], the stability of the system, lasing phonon statistics and the threshold still need to be rigorously analyzed. Motivated by the experiment on phonon lasing [30] and considering both theoretical [32–38] and experimental [39, 40] studies on the coupled optomechanical systems from optical to microwave frequencies [13, 41], we have analyzed phonon lasing in coupled optomechanical systems by using a completely quantum theoretical approach.

*Electronic address: yuxiliu@mail.tsinghua.edu.cn

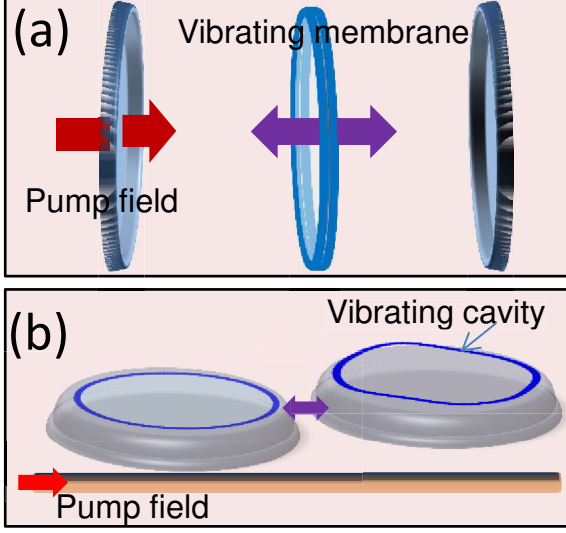


FIG. 1: (Color online) (a) A movable mirror is placed inside a cavity, and is coupled to the optical modes a_L and a_R of the left and right cavity. (b) A cavity is coupled to an optomechanical system. In both cases, we assume that the two cavity fields have the same frequencies and decay rates. A classical driving field is applied to the left cavity.

Our paper is organized as follows. In Sec. II, we give the Hamiltonian which is used to describe possible experimental setups, and then obtain the supermode description for the phonon lasing. In Sec. III, we derive the steady state solution using the equations of motion for the variables of the cavity fields and the mechanical resonator. We also study how the phonon number, population inversion of the supermodes, and pump power change with the driving field. In Sec. IV, we carefully study the phase diagram of the phonon lasing by using equations of motion in the phonon stimulated regime. In Sec. V, the phonon statistics is studied. Finally, we summarize and discuss our results.

II. THEORETICAL MODEL

As schematically shown in Fig. 1, we study two very similar systems: The first one contains a vibrating dielectric membrane (e.g., in Ref. [42]), which is placed midway between two mirrors as in Fig. 1(a), the Hamiltonian of the system is described in Refs. [32–35]; the second one consists of a cavity, which is coupled to an optomechanical system (e.g., in Ref. [30]) as in Fig. 1(b), the Hamiltonian of the system is described as in Refs. [36–38]. The difference between these systems is as follows. In the first system, both the left and the right cavity fields interact with the mechanical resonator, whereas in the second system only the right cavity field interacts with the mechanical resonator. Besides a factor of $1/2$ difference in the coupling strength between the supermodes and the mechanical resonator described below in Eq. (1), we

find that two systems have the same Hamiltonian in the presentation of the supermodes. Thus we only deal with the Hamiltonian corresponding to Fig. 1 (a) in the following calculations.

We assume that the classical pump field with the frequency ω_d is applied to the left cavity and the two cavities have the same frequencies ω_c when the mechanical resonator is in its equilibrium position. We define the annihilation (creation) operators for the left and the right cavity fields as a_L (a_L^\dagger) and a_R (a_R^\dagger). By using the supermode operators $a_1 = (a_L + a_R)/\sqrt{2}$ and $a_2 = (a_L - a_R)/\sqrt{2}$ as in Ref. [30], the Hamiltonian H_0 for both systems driven by the external field can be written as

$$H_0 = \hbar\omega_m b^\dagger b - \hbar\chi \left(a_1^\dagger a_2 b + a_2^\dagger a_1 b^\dagger \right) + \hbar(g - \Delta) a_1^\dagger a_1 - \hbar(g + \Delta) a_2^\dagger a_2 + \frac{i\hbar}{\sqrt{2}} \left[\Omega(a_1^\dagger + a_2^\dagger) - \text{h.c.} \right], \quad (1)$$

with the frequencies $g - \Delta$ and $g + \Delta$ for supermodes 1 and 2. Here, χ represents the coupling strength between the cavity field and the mechanical resonator via the radiation pressure. We note that χ should be changed into $\chi/2$ for the system shown in Fig. 1(b). $\Delta = \omega_d - \omega_c$ is the detuning between the driving field and cavity mode. b and b^\dagger denote the annihilation and creation operators of the mechanical mode with the frequency ω_m . The interaction strength between the two cavities is described by the parameter g . The coupling constant between the driving field and the left cavity field is Ω .

Using the Hamiltonian in Eq. (1) and also considering the environmental effect, we can obtain equations of motion for all variables of the system as

$$\frac{da_1}{dt} = - \left[\frac{\gamma_c}{2} + i(g - \Delta) \right] a_1 + i\chi a_2 b + \frac{\Omega}{\sqrt{2}} + \Gamma_1(t), \quad (2)$$

$$\frac{da_2}{dt} = - \left[\frac{\gamma_c}{2} - i(g + \Delta) \right] a_2 + i\chi a_1 b^\dagger + \frac{\Omega}{\sqrt{2}} + \Gamma_2(t), \quad (3)$$

$$\frac{db}{dt} = - (\gamma_m + i\omega_m) b + i\chi a_2^\dagger a_1 + \sqrt{2\gamma_m} b_{\text{in}}. \quad (4)$$

Here, we assume that decay rates γ_L and γ_R of the left and right cavities are same, i.e., $\gamma_L \equiv \gamma_R = \gamma_c$, and the decay rate of the mechanical resonator is assumed as γ_m . $\Gamma_1(t)$, $\Gamma_2(t)$, and $b_{\text{in}}(t)$ represent fluctuation operators corresponding to the supermodes and the mechanical resonator. As shown in Appendix A, the correlation functions of the fluctuation operators of the supermodes in the time domain under the Markovian approximation are given as

$$\langle \Gamma_1(t) \Gamma_1^\dagger(t') \rangle = \langle \Gamma_2(t) \Gamma_2^\dagger(t') \rangle = \gamma_c \delta(t - t'), \quad (5)$$

$$\langle \Gamma_1^\dagger(t) \Gamma_1(t') \rangle = \langle \Gamma_2^\dagger(t) \Gamma_2(t') \rangle = 0. \quad (6)$$

Here, we assume that the thermal energy due to environmental temperature T is sufficiently lower than the transition energies of the supermodes, thus the effect of the environmental temperature on two supermodes is negligibly small. We assume that the frequency of the mechanical resonator is low, thus the temperature effect on the mechanical resonator should be included. That is, the correlation functions of the fluctuation

operators of the mechanical resonator is assumed as

$$\langle b_{\text{in}}^\dagger(t)b_{\text{in}}(t') \rangle = n_b(T)\delta(t-t'), \quad (7)$$

$$\langle b_{\text{in}}(t')b_{\text{in}}^\dagger(t) \rangle = [n_b(T) + 1]\delta(t-t'), \quad (8)$$

where $n_b(T) = 1/[\exp(\hbar\omega_m/K_B T) - 1]$ denotes the thermal phonon number of the mechanical resonator, with the Boltzmann constant K_B .

III. STEADY STATES ANALYSIS

In this section, we analyze the steady-state of the coupled optomechanical systems. First, we show that the bistable behavior can be observed in these coupled systems even in the blue detuning regime. Then, we analyze the stability under small disturbances in the parameter regions of phonon coherent amplification.

A. Mechanical bistability

By using the semiclassical approximation, e.g., $\langle a_2 b \rangle = \langle a_2 \rangle \langle b \rangle$, we obtain the average value of the Eqs.(2)-(4) as

$$\langle \dot{a}_1 \rangle = - \left[\frac{\gamma_c}{2} + i(g - \Delta) \right] \langle a_1 \rangle + i\chi \langle a_2 \rangle \langle b \rangle + \frac{\Omega}{\sqrt{2}}, \quad (9)$$

$$\langle \dot{a}_2 \rangle = - \left[\frac{\gamma_c}{2} - i(g + \Delta) \right] \langle a_2 \rangle + i\chi \langle a_1 \rangle \langle b^\dagger \rangle + \frac{\Omega}{\sqrt{2}}, \quad (10)$$

$$\langle \dot{b} \rangle = -\gamma_m \langle b \rangle - i\omega_m \langle b \rangle + i\chi \langle a_2^\dagger \rangle \langle a_1 \rangle. \quad (11)$$

Defining the steady state values of the cavity fields and the mechanical resonator as $\langle a_1 \rangle_s = A_1$, $\langle a_2 \rangle_s = A_2$, and $\langle b \rangle_s = B_0$ respectively, and then setting $\langle a_1 \rangle_s = \langle a_2 \rangle_s = \langle b \rangle_s = 0$, we obtain the following relation between the driving strength Ω and the mechanical mode B_0

$$|\Omega|^2 = \frac{2B_0(\gamma_m + i\omega_m) \left[(|\xi|^2 - \Delta^2 + \chi^2|B_0|^2)^2 + \gamma_c^2\Delta^2 \right]}{i\chi \left[\xi^2 + (\chi B_0 - \Delta)^2 \right]}, \quad (12)$$

where we have defined $\xi = \gamma_c/2 - ig$. As shown in Fig. 2, the red solid curve represents the stable region of phonon mode, while blue dashed curve represents the boundary between stable and unstable regions. When the strength of driving field is increased to a critical point, the system becomes unstable and the bistability behaviors of phonon mode can be observed. In contrast to the results of single-mode optomechanical system where bistability can be shown only in the red-detuning regime [43], the bistability of coupled optomechanical systems can be observed in the blue-detuning regime.

From Fig. 2, we see that the curve of the steady-state value $|B_0|$ of the phonon mode versus the strength of the driving field $|\Omega|$ is not in the usual S-shape. This is because the driving field is now in the strong regime which leads to so called unconventional bistability behaviors [44].

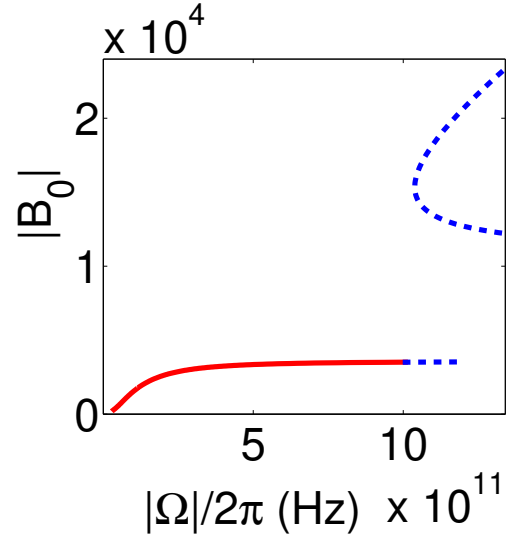


FIG. 2: (Color online) The steady-state value $|B_0|$ is plotted as function of the strength $|\Omega|/(2\pi)$ of driving field. The other parameters are assumed as $\omega_m/(2\pi) = 23.4$ MHz, $\chi/(2\pi) = 1570$ Hz, $\gamma_m/(2\pi) = 0.125$ MHz, $\gamma_c/(2\pi) = 4.8$ MHz, $g/(2\pi) = 11.7$ MHz, and $\Delta = g/2$.

B. Stabilities

To discuss the stability of the system against small perturbations, let us now express the variables a_1 , a_2 , and b as the sums of their stable steady-state values and small fluctuations, that is,

$$a_1(t) = A_1 + \Lambda_1(t), \quad (13)$$

$$a_2(t) = A_2 + \Lambda_2(t), \quad (14)$$

$$b(t) = B_0 + \beta(t). \quad (15)$$

The expressions of $a_1^\dagger(t)$, $a_2^\dagger(t)$ and $b^\dagger(t)$ can be obtained from the Hermitian conjugates of $a_1(t)$, $a_2(t)$ and $b(t)$ correspondingly. Here, the average values of fluctuation terms are zero, i.e., $\langle \Lambda_1^\dagger(t) \rangle = \langle \Lambda_2^\dagger(t) \rangle = \langle \beta(t) \rangle = 0$. The steady-state values A_1 , A_2 , B_0 and their complex conjugates can be easily obtained from Eqs. (9)-(11) by setting all time derivatives to zero. Then we can write down the linearized dynamical equations of the fluctuation terms up to the first order as

$$\frac{d}{dt} \vec{u} = M \vec{u}. \quad (16)$$

Here, the matrix M is given as

$$M = i\chi \begin{pmatrix} \frac{\epsilon_1}{i\chi} & 0 & B_0 & 0 & A_2 & 0 \\ 0 & \frac{\epsilon_1^*}{i\chi} & 0 & -B_0^* & 0 & -A_2^* \\ B_0^* & 0 & \frac{\epsilon_2}{i\chi} & 0 & 0 & A_1 \\ 0 & -B_0 & 0 & \frac{\epsilon_2^*}{i\chi} & -A_1^* & 0 \\ A_2^* & 0 & 0 & A_1 & \frac{\epsilon_3}{i\chi} & 0 \\ 0 & -A_2 & -A_1^* & 0 & 0 & \frac{\epsilon_3^*}{i\chi} \end{pmatrix} \quad (17)$$

with $\epsilon_1 = -(\gamma_c/2) - i(g - \Delta)$, $\epsilon_2 = -(\gamma_c/2) + i(g + \Delta)$, and $\epsilon_3 = -\gamma_m - i\omega_m$. The vector \vec{u} in Eq. (16) is defined as

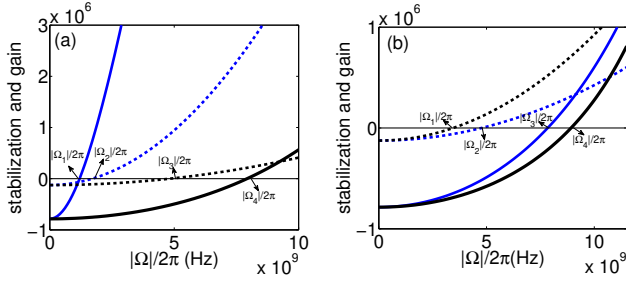


FIG. 3: (Color online) The real part of the eigenvalues $\text{Re}(\lambda)$ of the matrix M in Eq. (17) and the net gain α' in Eq. (26) of phonons versus the strength $|\Omega|$ of the driving field. Solid curves describe $\text{Re}(\lambda)$, and the dashed curves correspond to α' . (a) Blue curves correspond to $\Delta = g$, while the black curves correspond to $\Delta = g/2$. We set $\gamma_c/(2\pi) = 4.8$ MHz. The points $|\Omega_1|/(2\pi)$ and $|\Omega_4|/(2\pi)$ correspond to $\text{Re}(\lambda) = 0$, however $|\Omega_2|/(2\pi)$ and $|\Omega_3|/(2\pi)$ correspond to $\alpha' = 0$. (b) The blue curves correspond to $\gamma_c/(2\pi) = 4.8$ MHz, while the black curves correspond to $\gamma_c/(2\pi) = 2.8$ MHz. Here, we set $\Delta = g/2$. The points $|\Omega_3|/(2\pi)$ and $|\Omega_4|/(2\pi)$ correspond to $\text{Re}(\lambda) = 0$, whereas $|\Omega_1|/(2\pi)$ and $|\Omega_2|/(2\pi)$ correspond to $\alpha' = 0$. The other parameters are the same as in Fig. 2 except coupling strength g between two cavities, its value can be obtained from the quantity $\delta/(2\pi) = (2g - \omega_m)/(2\pi) = 1$ MHz.

$\vec{u} = (\Lambda_1 \Lambda_1^\dagger \Lambda_2 \Lambda_2^\dagger \beta \beta^\dagger)^T$ where the superscript T denotes the transpose.

The stability of the system is determined by the eigenvalues of the matrix M . If the real parts of the eigenvalues of M are all negative, the system is stable. Otherwise the system is unstable. It is not easy to analytically solve the eigenvalues of M . However, we can numerically calculate them. The matrix M includes three pairs of conjugate eigenvalues, we find that the real parts of two pairs of eigenvalues are always negative near the threshold, thus we need only to calculate the real part $\text{Re}(\lambda)$ of the eigenvalues for the remaining pair. In Fig. 3, the real parts $\text{Re}(\lambda)$ of these two eigenvalues as a function of the strength $|\Omega|$ of the driving field is plotted for given parameters. From Fig. 3(a), we find that the system has a larger stable region, i.e., $\text{Re}(\lambda) < 0$, for the strength $|\Omega|$ of the driving field in the case $\Delta = g/2$ in contrast to $\Delta = g$. Figure 3(b) shows that the stable region of the system becomes smaller for faster decay rates of the cavity field. As a comparison with the stability of the system, the gain of the phonon lasing is also plotted as a function of the strength $|\Omega|$ of the driving field in Fig. 3. The detailed discussion will be given when Eq. (26) is introduced.

IV. PHONON LASING

Let us now discuss the important properties of the phonon lasing. Under the adiabatic approximation of angular operators of supermodes, we derive the dynamical equation of the phonon mode and revisit the threshold condition of phonon lasing which was obtained in Ref. [30]. We also define an effective potential for the phonon mode near the threshold in a special case, and discuss the phase diagram of phonon lasing.

A. Phonon lasing equation and threshold condition

To find the relation between the phonon lasing and population inversion of two supermodes, and also to compare the phonon lasing with the photon lasing generated by two-level atomic system, we define the ladder and population inversion operators via the angular momentum operators constructed by two bosonic supermode operators [45]. Because the energy of the supermode 1 is larger than that of the supermode 2, then we define the angular momentum operators as: $J_+ = a_1^\dagger a_2$, $J_- = a_2^\dagger a_1$ and $J_z = (a_1^\dagger a_1 - a_2^\dagger a_2)/2$. It is clear that J_+ and J_- are ladder operators, while J_z describes the population inversion from the supermode mode 1 to 2.

Using Eqs. (2)-(4) and also their Hermitian conjugates, the dynamical equations for the variables J_- and J_z can be obtained as below

$$\begin{aligned} \frac{dJ_-}{dt} &= -\gamma_c J_- - 2igJ_- - 2i\chi J_z b + \frac{\Omega^*}{\sqrt{2}} a_1 + \frac{\Omega}{\sqrt{2}} a_2^\dagger \\ &+ \Gamma_2^\dagger(t) a_1 + a_2^\dagger \Gamma_1(t), \end{aligned} \quad (18)$$

$$\begin{aligned} \frac{dJ_z}{dt} &= -\gamma_c J_z + i\chi J_+ b - i\chi J_- b^\dagger + \frac{\Omega}{2\sqrt{2}} a_1^\dagger + \frac{\Omega^*}{2\sqrt{2}} a_1 \\ &- \frac{\Omega}{2\sqrt{2}} a_2^\dagger - \frac{\Omega^*}{2\sqrt{2}} a_2 + \frac{1}{2} a_1^\dagger \Gamma_1(t) + \frac{1}{2} \Gamma_1^\dagger(t) a_1 \\ &- \frac{1}{2} a_2^\dagger \Gamma_2(t) - \frac{1}{2} \Gamma_2^\dagger(t) a_2, \end{aligned} \quad (19)$$

$$\frac{db}{dt} = -\gamma_m b - i\omega_m b + i\chi J_- + \sqrt{2\gamma_m} b_{in}(t). \quad (20)$$

Here, we note that unpaired operators of the optical supermodes are still remained in Eqs. (18) and (19). Eqs (18)-(20) for the optical supermodes interacting with the phonon mode are very similar to those of photon lasing [46]. However, we can also easily find the difference between the phonon lasing, described in Eqs. (18) and (19), and the photon lasing in a two-level system [46]. Since additional terms $(\Omega^* a_1 + \Omega a_2^\dagger)/\sqrt{2}$ appear in Eq. (18) and $[\Omega^*(a_1 - a_2) + \text{h.c.}]/2\sqrt{2}$ in Eq. (19), the phonon lasing studied here will show different behaviors compared to the photon lasing with two-level systems [46].

We assume that the decay rate γ_c of the cavity field is much larger than the decay rate γ_m of the mechanical resonator, then the variables J_- and J_z of the cavity field will be subject to the dynamics of the mechanical resonator under the conditions that $\partial J_-/(\gamma_c \partial t) \ll J_-$ and $\partial J_z/(\gamma_c \partial t) \ll J_z$ which leads to the so-called adiabatical approximation. By setting $\partial J_-/\partial t = 0$ and $\partial J_z/\partial t = 0$, we can obtain the expression of J_- and J_z . Substituting the expression of J_- into the dynamical equation of b in Eq. (20), we have

$$\begin{aligned} \frac{db}{dt} &= -i\omega_m b - \left[\gamma_m - 2 \frac{\chi^2 J_z}{\gamma_c + i\delta} \right] b + \frac{\alpha}{\sqrt{2}} (\Omega^* a_1 + \Omega a_2^\dagger) \\ &+ \alpha \left[\Gamma_2^\dagger(t) a_1 + a_2^\dagger \Gamma_1(t) \right] + \sqrt{2\gamma_m} b_{in}(t), \end{aligned} \quad (21)$$

where $\alpha = i\chi/(\gamma_c + i\delta)$ and $\delta = 2g - \omega_m$ is a small detuning between two-level system formed by supermodes and the

frequency of the mechanical resonator (see the fast oscillating term $i2gJ_-$ in Eq. (18)). From Eq. (21), we find the phonon lasing gain as

$$G' = \text{Re} \left(\frac{2\chi^2 J_z}{\gamma_c + i\delta} \right) = \frac{2\chi^2 \gamma_c J_z}{\gamma_c^2 + (2g - \omega_m)^2} \quad (22)$$

if we omit the single mode terms related to a_1 and a_2 in Eq. (21). We note that this is just the phonon lasing gain obtained in Ref. [30]. The gain described by Eq. (22) is not so simple when the third term of the right hand of Eq. (21) is taken into account.

To obtain more exact expression for the gain of phonon lasing, let us further adiabatically eliminate a_1 and a_2 in Eq. (21) by setting $\partial a_i / \partial t = 0$ (with $i = 1, 2$) in Eqs. (2) and (3). In this case, equation (21) can be reexpressed as

$$\begin{aligned} \frac{db}{dt} = & - \left[\gamma_m - \frac{2\chi^2 J_z}{\gamma_c + i\delta} + \frac{i\Delta\gamma_c\chi^2|\Omega|^2}{(\gamma_c + i\delta)(N^2 + \Delta^2\gamma_c^2)} \right] b \\ & - i\omega_m b + i \frac{\chi|\Omega|^2 [N(\gamma_c - i2g) + 2\Delta^2\gamma_c]}{2(\gamma_c + i\delta)(N^2 + \Delta^2\gamma_c^2)} + \Gamma(t), \end{aligned} \quad (23)$$

where the parameter N is defined as $N = \gamma_c^2/4 + g^2 - \Delta^2 + \chi^2 b^\dagger b$; and the noise term $\Gamma(t)$ can be found in Eq. (A9) in Appendix A. Thus, the gain G of the phonon lasing from Eq. (23) becomes

$$G = G' - \frac{\Delta\delta\gamma_c\chi^2|\Omega|^2}{(\gamma_c^2 + \delta^2)(N^2 + \Delta^2\gamma_c^2)} \quad (24)$$

where G' is the same as G' given in Eq. (22). It is clear that the gain is proportional to the population inversion J_z when $\Delta = \omega_d - \omega_c = 0$. However, the gain becomes complicated when $\omega_d \neq \omega_c$. From Eq. (23), we can obtain the threshold condition $\gamma_m = G$, that is, the phonon can be amplified when $G > \gamma_m$. We can see from Eq. (24) that the threshold condition in Ref. [30] is valid only when the cavity field is resonantly driven.

B. Phase diagram for phonon lasing

To sketch the phase diagram of the phonon lasing, we further express J_z in Eq. (23) as the variables of mechanical mode by adiabatically eliminating the degrees of freedom of the cavity mode. As a result we can express J_z as the function of phonon operators in the regime close to the threshold such that $n \ll (\gamma_c^2 + \delta^2)/4\chi^2$ (see Eq. (B3) in Appendix B).

By replacing J_z in Eq. (21) by Eq. (B3), we obtain

$$\frac{db}{dt} = G_0 + G_1 b + G_2 b^\dagger b + G_3 b b - G_4 b^\dagger b b, \quad (25)$$

up to third-order terms of the operator b near the threshold value of the phonon lasing. The coefficients G_i (for $i = 0, 1, \dots, 4$) can be found from Eqs. (B7) to (B11) in Appendix B. By calculating the real part of G_1 , the net gain of phonon can be given as,

$$\alpha' = \eta_3 - \gamma_m. \quad (26)$$

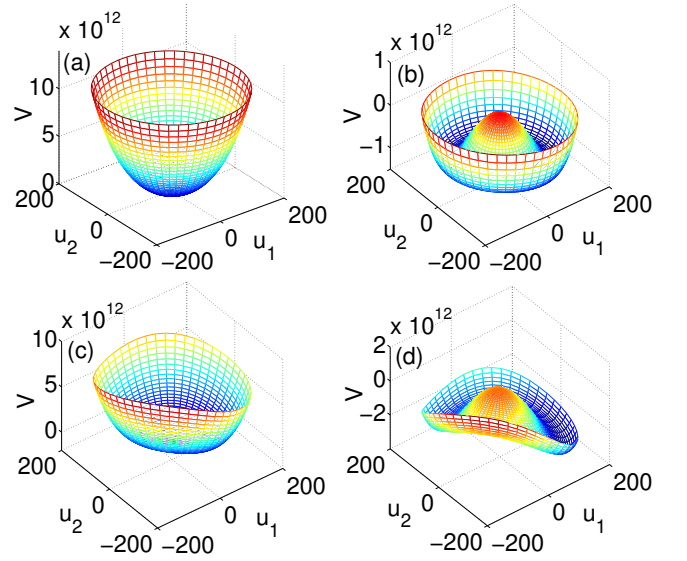


FIG. 4: (Color online) The two-dimensional scalar potential V as functions of u_1 and u_2 . The parameters corresponding to four figures are: (a) $\eta_1/(2\pi) = 100$ MHz, $\eta_2/(2\pi) = 50$ MHz, $\alpha'/(2\pi) = -50$ MHz, $\text{Im}(G_1)/(2\pi) = -1$ MHz, $\varepsilon_6/(2\pi) = 2000$ Hz, $\eta_7/(2\pi) = 1800$ Hz, and $\eta_8/(2\pi) = 10$ Hz; (b) $\alpha'/(2\pi) = 36$ MHz, and the other parameters are the same as in (a); (c) $\eta_1/(2\pi) = 1$ GHz, $\eta_2/(2\pi) = 0.5$ GHz, $\alpha'/(2\pi) = -5$ MHz, $\text{Im}(G_1)/(2\pi) = -20$ MHz, $\varepsilon_6/(2\pi) = 0.02$ MHz, $\eta_7/(2\pi) = 2500$ Hz, and $\eta_8/(2\pi) = 100$ Hz; (d) $\alpha'/(2\pi) = 20$ MHz, and the other parameters are the same as in (c).

The definitions of η_i (for $i = 1, 2, \dots, 8$) are defined in Eqs. (B12)-(B19) in Appendix B.

In Fig. 3, the variations of the gain α' as a function of the strength $|\Omega|$ of the driving field is plotted. If the value of α' is positive, the phonon lasing can be realized. Moreover, the phonon lasing also requires that the system is in the stable region. From Fig. 3(a), we find that the region with both $\alpha' > 0$ and $\text{Re}(\lambda) < 0$, which is for a stable phonon lasing, is smaller for $\Delta = g$ than that for $\Delta = g/2$. That is, the region between $|\Omega_1|/(2\pi)$ and $|\Omega_2|/(2\pi)$ is smaller than that between $|\Omega_3|/(2\pi)$ and $|\Omega_4|/(2\pi)$. From Fig. 3(b), we also find that the decay rate of the cavity field affects both the stability and the gain. It is seen that smaller decay rate γ_c of the cavity field leads to a larger region for stable phonon lasing, that is, the region between $|\Omega_1|/(2\pi)$ and $|\Omega_4|/(2\pi)$ corresponding to $\gamma_c/(2\pi) = 2.8$ MHz is larger than that between $|\Omega_2|/(2\pi)$ and $|\Omega_3|/(2\pi)$ corresponding to $\gamma_c/(2\pi) = 4.8$ MHz.

With the semi-classical approximation, the phonon field b can be written as a two-dimensional vector $b = (u_1 \ u_2)^T$ with $u_1 = \text{Re}(b)$ and $u_2 = \text{Im}(b)$. Thus, we can obtain the dynamical equations for u_1 and u_2 as shown in Eqs. (B20) and (B21) of Appendix B. We should note here that it is usually difficult to define a scalar potential for the mechanical mode.

We now discuss a special case with $\delta = 0$. In this case, the equations of motion for u_1 and u_2 are given as in Eqs. (B26) and (B27). When $u_1 \gg u_2$, the terms containing u_2 are much smaller than the same order terms including u_1 , then we can

approximately define a two-dimensional scalar potential

$$V \approx -\eta_1 u_1 - \eta_2 u_2 + \text{Im}(G_1)u_1 u_2 - \frac{\alpha'}{2}(u_1^2 + u_2^2) - \frac{\varepsilon_6}{3}u_1^3 + \frac{\eta_7}{4}(u_1^2 + u_2^2)^2 - \eta_8 u_1^3 u_2 - \frac{\eta_8}{3}u_2^3 u_1. \quad (27)$$

The definition of ε_6 can be found in Eq. (B22) in Appendix B. Actually, in other parameter regimes, e.g., a larger δ , we may also have $u_2 \gg u_1$, and the scalar potential similar to Eq. (27) can also be obtained.

In Fig 4, the two-dimensional scalar potential V is plotted as functions of u_1 and u_2 . We find that when the coefficients η_1 , η_2 and ε_7 are negligibly small, the potential V approximately has a rotating symmetry in the u_1 - u_2 plane, otherwise, the symmetry is broken. It is also easily found that the potential V has only one equilibrium point given at $b = (u_1, u_2) = 0$ when $\alpha' < 0$, that is, there is no phonon lasing (In fact, it is possible to have nonzero equilibrium points for V if the value of α' is negative but very close to 0). However if $\alpha' > 0$, $b = 0$ is not a stable point. Instead, two new stable points appear. We find that these two stable points are not symmetric for the nonzero coefficients of odd terms of u_1 and u_2 (in Eq. (27)) in contrast to the case of photon lasing [46] in which two stable points are always symmetric. We note that Eq. (25) is valid only near the threshold.

In the case that the terms including u_2 in V are negligibly smaller than the terms including u_1 , then we can neglect all terms including u_2 ($u_1 \gg u_2$) in Eq. (27) and approximately define the one-dimensional scalar potential

$$V = -\eta_1 u_1 - \frac{\alpha'}{2}u_1^2 - \frac{\varepsilon_6}{3}u_1^3 + \frac{\eta_7}{4}u_1^4. \quad (28)$$

In Fig. 5, V is plotted as a function of u_1 according to Eq. (28). We also show in Fig. 5 that the shape of the potential function V changes from the parabolic potential well to two symmetric potential wells, and then to two asymmetric potential wells as the parameters are varied. Actually, potential similar to that given in Fig. 5 can also be found for u_2 in some parameter regimes.

V. STATISTICAL PROPERTIES OF THE PHONON

We now study the statistical properties of the phonons by calculating the second-order degrees of coherence in the same way as usually done for photons [31]. The normalized equal-time second-order correlation function of the phonons is defined as $g_2(0) = \langle b^\dagger(t)b^\dagger(t)b(t)b(t) \rangle / \langle b^\dagger(t)b(t) \rangle^2$. Using the small-fluctuation approximation as shown in Eqs. (13)-(15), the degree of second-order coherence can be written as

$$g_2(0) = \frac{|B_0|^4 + 2\text{Re}[B_0^{*2}\langle\beta(t)\beta(t)\rangle] + 4|B_0|^2\langle\beta^\dagger(t)\beta(t)\rangle}{(|B_0|^2 + \langle\beta^\dagger(t)\beta(t)\rangle)^2} + \frac{\langle\beta^\dagger(t)\beta^\dagger(t)\beta(t)\beta(t)\rangle}{(|B_0|^2 + \langle\beta^\dagger(t)\beta(t)\rangle)^2}. \quad (29)$$

If the phonon mode is in the coherent state, the value of $g_2(0) = 1$.

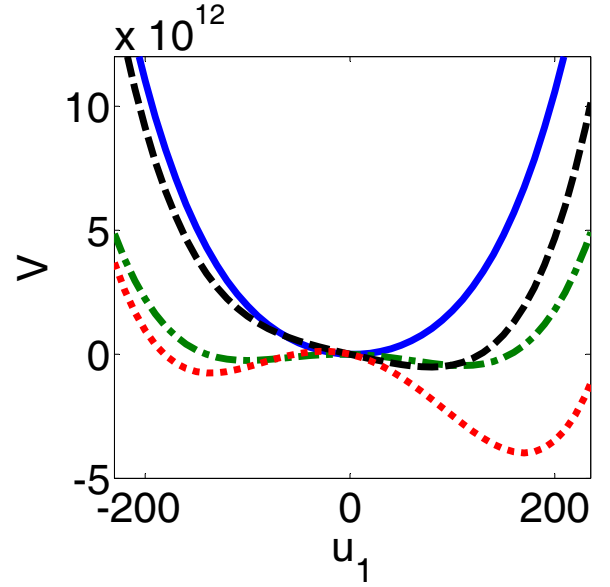


FIG. 5: (Color online) One dimensional potential V as a function of u_1 . The parameters corresponding to four curves are: (a) $\eta_1/(2\pi) = 100$ MHz, $\alpha'/(2\pi) = -50$ MHz, $\varepsilon_6/(2\pi) = 2000$ Hz, and $\eta_7/(2\pi) = 1800$ Hz (blue solid curve); (b) $\alpha'/(2\pi) = 36$ MHz, the other parameters are the same as in (a) (green dash-dotted curve); (c) $\eta_1/(2\pi) = 1$ GHz, $\alpha'/(2\pi) = -5$ MHz, $\varepsilon_6/(2\pi) = 0.02$ MHz, and $\eta_7/(2\pi) = 2500$ Hz (black dashed curve); (d) $\alpha'/(2\pi) = 20$ MHz, the other parameters are the same as in (c) (red dotted curve).

It is somewhat difficult to calculate the fluctuation operator $\beta(t)$ in the time domain, thus we try to calculate it in the frequency domain. By introducing the Fourier transform, we can obtain the dynamical equation for the fluctuation operators in the frequency domain as in Eqs. (C4)-(C6) of Appendix C. In this case, we can obtain the phonon fluctuation operators in the frequency domain as follows

$$\begin{aligned} \tilde{\beta}(\omega) &= p_1(\omega)\tilde{b}_{\text{in}}(\omega) + p_2(\omega)\tilde{b}_{\text{in}}^\dagger(\omega) + p_3(\omega)\tilde{\Gamma}_1(\omega) \\ &+ p_4(\omega)\tilde{\Gamma}_1^\dagger(\omega) + p_5(\omega)\tilde{\Gamma}_2(\omega) + p_6(\omega)\tilde{\Gamma}_2^\dagger(\omega). \end{aligned} \quad (30)$$

The parameters p_i ($i = 1, 2, \dots, 6$) in Eq. (30) are given from Eqs. (C7)-(C12) in Appendix C. From Eqs. (5)-(8), the correlation functions of the input noise operators in the frequency domain can be easily obtained. Then, from Eq. (30), we can obtain the correlation functions of the phonon fluctuation operators in the frequency domain as follows

$$\langle \tilde{\beta}(\omega)\tilde{\beta}(\omega') \rangle = 2\pi\Gamma_{\beta\beta}\delta(\omega + \omega'), \quad (31)$$

$$\langle \tilde{\beta}^\dagger(\omega)\tilde{\beta}(\omega') \rangle = 2\pi\Gamma_{\beta^\dagger\beta}\delta(\omega + \omega'). \quad (32)$$

with the coefficients defined as

$$\begin{aligned} \Gamma_{\beta\beta}(\omega) &= p_1(\omega)p_2(-\omega)(n_b + 1) + p_2(\omega)p_1(-\omega)n_b \\ &+ p_3(\omega)p_4(-\omega)\gamma_c + p_5(\omega)p_6(-\omega)\gamma_c, \end{aligned} \quad (33)$$

$$\begin{aligned} \Gamma_{\beta^\dagger\beta}(\omega) &= |p_1(-\omega)|^2 n_b + |p_2(-\omega)|^2 (n_b + 1) \\ &+ |p_4(-\omega)|^2 \gamma_c + |p_6(-\omega)|^2 \gamma_c. \end{aligned} \quad (34)$$

Here, $\Gamma_{\beta\beta}(\omega)$ and $\Gamma_{\beta^\dagger\beta}(\omega)$ represent the correlation spectra of the phonon fluctuation operators. If we assume that

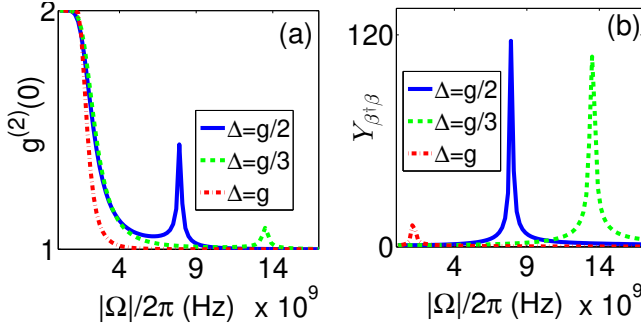


FIG. 6: (Color online) The degree of second-order coherence $g^{(2)}(0)$ in (a) and the phonon number fluctuation $Y_{\beta\ddagger\beta}$ in (b) as the functions of the strength $|\Omega|$ of the driving field. The three curves correspond to different detunings: (1) $\Delta = g/2$ (blue solid curve); (2) $\Delta = g/3$ (green dashed curve); (3) $\Delta = g$ (red dash-dotted curve). The other parameters are the same as in Fig. 2 except $T = 1$ mK.

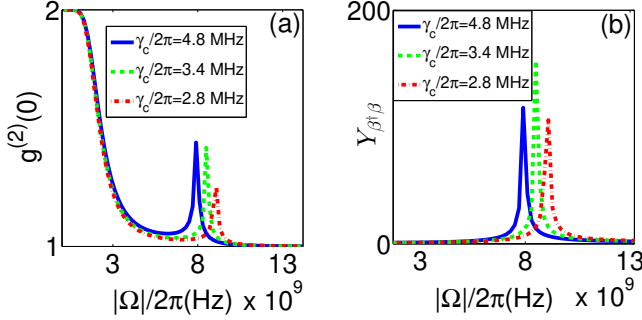


FIG. 7: (Color online) The degree of second-order coherence $g^{(2)}(0)$ in (a) and the phonon number fluctuation $Y_{\beta\ddagger\beta}$ in (b) as the function of the strength $|\Omega|$ for the driving field. The three curves correspond to different cavity decay rates: (1) $\gamma_c/(2\pi) = 4.8$ MHz (blue solid curve); (2) $\gamma_c/(2\pi) = 3.4$ MHz (green dashed curve); (3) $\gamma_c/(2\pi) = 2.8$ MHz (red dash-dotted curve). The other parameters are the same as in Fig. 2 except $\Delta = g/2$ and $T = 1$ mK.

the environmental noises have Gaussian distributions, then, from Wick's theorem, all higher-order correlation functions can be written as the combinations of the first- and second-order correlation functions [47]. Thus, with straightforward but tedious calculations, we have $\langle \beta^\dagger(t)\beta^\dagger(t)\beta(t)\beta(t) \rangle = 2Y_{\beta\ddagger\beta}^2 + |Y_{\beta\beta}|^2$, where $Y_{\beta\beta}$ and $Y_{\beta\ddagger\beta}$ can be calculated as

$$Y_{\beta\beta} = \langle \beta(t)\beta(t) \rangle = \frac{1}{2\pi} \int_{-\infty}^{+\infty} \Gamma_{\beta\beta}(\omega) d\omega, \quad (35)$$

$$Y_{\beta\ddagger\beta} = \langle \beta^\dagger(t)\beta(t) \rangle = \frac{1}{2\pi} \int_{-\infty}^{+\infty} \Gamma_{\beta\ddagger\beta}(\omega) d\omega. \quad (36)$$

The degree of second-order coherence $g^{(2)}(0)$ for the phonons is plotted as a function of the strength Ω of the driving field for different detunings Δ , cavity decay rates γ_c , and temperatures T in Fig. 6(a), Fig. 7(a), and Fig. 8(a), respectively. All three figures show $g^{(2)}(0) = 2$ when the driving field is not applied to the cavity. This means that the phonons are in the thermal equilibrium state. However, when the driving field strength Ω approaches to (or is above) the threshold,

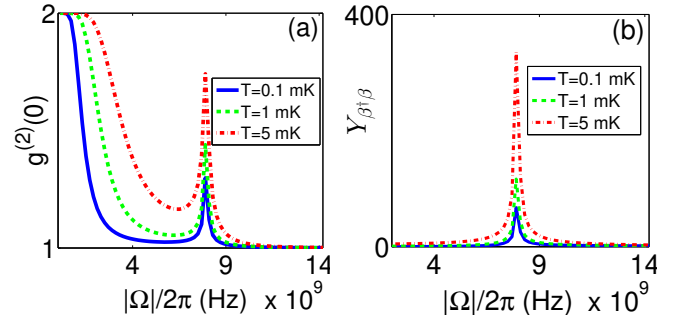


FIG. 8: (Color online) The degree of second-order coherence $g^{(2)}(0)$ in (a) and the phonon number fluctuation $Y_{\beta\ddagger\beta}$ in (b) as the function of the strength $|\Omega|$ for the driving field. The three curves correspond to different temperatures: (1) $T = 0.1$ mK (blue solid curve); (2) $T = 1$ mK (green dashed curve); (3) $T = 5$ mK (red dash-dotted curve). The other parameters are the same as in Fig. 2 except $\Delta = g/2$.

the degree of coherent $g^{(2)}(0)$ quickly approaches to (or is) 1, which means that the phonon is in a coherent state and the phonon lasing occurs.

In contrast to $g^{(2)}(0) = 1$ in the photon lasing with two-level atoms [46], we find that there is a resonant peak in the curve of $g^{(2)}(0)$, the reason is that the spectrum $\Gamma_{\beta\ddagger\beta}(\omega)$ of phonon fluctuation operators is not only the function of frequency ω , but also the functions of the strength Ω for the driving field, cavity decay rate γ_c , the detuning Δ and so on. When the strength Ω of the driving field varies, the resonant peaks will appear in the spectrum $\Gamma_{\beta\ddagger\beta}(\omega)$, and then in the degree of second-order coherence. The correlation function $Y_{\beta\ddagger\beta}$, which is the inverse Fourier transform of $\Gamma_{\beta\ddagger\beta}(\omega)$, is plotted as a function of strength Ω of the driving field for different detunings Δ in Fig. 6(b), cavity decay rates γ_c in Fig. 7(b) and temperatures T in Fig. 8(b).

From Fig. 6 and Fig. 7, we find that the detuning Δ , cavity decay γ_c , and temperature T affect both the degree of second-order coherence and the correlation spectrum of phonon fluctuation operators. We also find that the positions and heights of the resonant peaks of $g^{(2)}(0)$ and $Y_{\beta\ddagger\beta}$ change when the parameters γ_c and Δ are varied. The temperature T , on the other hand, only affects the height of resonant peaks as shown in Fig. 8, and has no effect on their positions. With the increase of the temperature, the mechanical mode is gradually thermalized, and the coherent properties of phonon state degrade.

VI. CONCLUSIONS

In summary, we have theoretically analyzed the phonon lasing studied in Ref. [30] for a coupled optomechanical system. We have showed that in the steady-state the phonon mode shows unconventional bistability in the regime of strong driving field. We have derived the equations of phonon lasing by adiabatically eliminating the cavity modes, and then obtained the gain and threshold of the mechanical amplification.

We have found that the positive net gain of phonon lasing can be obtained in a stable regime, and thus it is possible to create stable coherent phonons in a coupled optomechanical system. In particular, we have clarified that the threshold given in Ref. [30] is just a special case for the phonon lasing in coupled optomechanical systems.

Interestingly, our study shows that the phonon lasing generated by photonic supermodes is somewhat different from the photon lasing generated by a two-level atomic system [31]. For example, even when there is no photon population inversion, the mechanical mode can be amplified. In contrast to the photon lasing, there is no saturation for phonon lasing. From the phase diagram of phonon lasing, we have found that a scalar potential can be approximately defined in some special cases. Different from photon lasing [31], the symmetry of the effective potential for phonon mode can be broken when the driving field is strong enough.

We have also studied the degree of second-order coherence of the phonon mode. We have showed that it tends to one when the driving field is strong enough. This means that the phonon mode reaches to a coherent state. Moreover, a resonant peak occurs in the degree of second-order coherence when the strength of the driving field satisfies certain conditions. This distinguished difference from the photon lasing [31] is due to the dependence of phonon fluctuation operators on the properties of the driving field. Our study have clarified some important points for phonon lasing in coupled optomechanical systems. We believe that our results will be useful in designing new experiments and in interpreting their results. In particular, they will be of great interest for the efforts to demonstrate phonon lasing in parity-time (PT-) symmetric optical and optomechanical systems [48–50].

VII. ACKNOWLEDGEMENT

This work is partially supported by the National Natural Science Foundation of China under Grant No. 61328502. Y.X.L. is supported by the NSFC under Grant No. 61025022 and the National Basic Research Program of China Grant No. 2014CB921401. J.Z. is supported by the NFSC under Grant Nos. 61174084, 61134008, 60904034. L.Y. and S.K.O. are partially supported by ARO grant No. W911NF-12-1-0026.

Appendix A: Derivation of the dynamical equations

We consider a multi-mode optomechanical system consisting of two optical modes and one mechanical mode. The total Hamiltonian including the environmental noises can be writ-

ten as follows

$$\begin{aligned}
H = & \hbar\omega_a a_L^\dagger a_L + \hbar\omega_a a_R^\dagger a_R + \hbar g (a_L^\dagger a_R + a_R^\dagger a_L) \\
& + \hbar\omega_m b^\dagger b - \hbar\chi (a_L^\dagger a_L - a_R^\dagger a_R) (b^\dagger + b) \\
& + i\hbar \left[\Omega \exp(-i\omega_d t) a_L^\dagger - h.c. \right] \\
& + \hbar \sum_i \omega_{bi} b_i^\dagger b_i + \hbar \sum_i (g_{bi} b b_i^\dagger + h.c.) \\
& + \hbar \sum_i \omega_i^{(L)} a_{Li}^\dagger a_{Li} + \hbar \sum_i (g_i^{(L)} a_{Li}^\dagger a_L + h.c.) \\
& + \hbar \sum_i \omega_i^{(R)} a_{Ri}^\dagger a_{Ri} + \hbar \sum_i (g_i^{(R)} a_{Ri}^\dagger a_R + h.c.) \quad (A1)
\end{aligned}$$

b^\dagger (or b) is the creation (or annihilation) operator of the phonon mode with frequency ω_m . a_L^\dagger (or a_L) and a_R^\dagger (or a_R) represent the creation (or annihilation) operators of the left and right cavity fields respectively, and the corresponding frequencies of the two bare cavities are both ω_a . χ is the coupling strength between the cavity field and the mechanical resonator, and the interaction strength between the two optical cavities is g . b_i^\dagger (or b_i) is the creation (or annihilation) operator of the i -th environmental noise mode coupled with the mechanical resonator with coupling strength g_{bi} . a_{Li}^\dagger (or a_{Li}) and a_{Ri}^\dagger (or a_{Ri}) are the creation (or annihilation) operators of i -th environmental noise mode coupled with the optical modes in the left and right cavities with coupling strengths $g_i^{(L)}$ and $g_i^{(R)}$. A classical driving field with frequency ω_d and amplitude Ω is injected into the left cavity. $\Delta = \omega_d - \omega_a$ is the detuning frequency between the driving field and the mode in the left cavity (bare frequency).

We redefine two new optical modes $a_1 = (a_L + a_R)/\sqrt{2}$ and $a_2 = (a_L - a_R)/\sqrt{2}$, then in a rotating reference frame given by the unitary operation

$$U = \exp \left\{ -i\omega_d \left[\sum_{i=1}^2 a_i^\dagger a_i + \sum_i (a_{Li}^\dagger a_{Li} + a_{Ri}^\dagger a_{Ri}) \right] t \right\}, \quad (A2)$$

the Hamiltonian can be rewritten as

$$\begin{aligned}
H_r = & H_0 + \hbar \sum_i \omega_{bi} b_i^\dagger b_i + \hbar \sum_i (g_{bi} b b_i^\dagger + h.c.) \\
& + \hbar \sum_i \omega_i^{(L)} a_{Li}^\dagger a_{Li} + \hbar \sum_i \omega_i^{(R)} a_{Ri}^\dagger a_{Ri} \\
& + (\hbar/\sqrt{2}) \sum_i \left[g_i^{(L)} a_{Li}^\dagger (a_1 + a_2) + h.c. \right] \\
& + (\hbar/\sqrt{2}) \sum_i \left[g_i^{(R)} a_{Ri}^\dagger (a_1 - a_2) + h.c. \right], \quad (A3)
\end{aligned}$$

with the Hamiltonian H_0 given in Eq. (1). Here we also use the rotating wave approximation.

With the Hamiltonian in Eq. (A3), we can obtain the

Heisenberg-Langevin equations of the total system as follows

$$\begin{aligned} \dot{a}_1 &= -i(g - \Delta)a_1 + i\chi a_2 b + \Omega/\sqrt{2} \\ &\quad - (i/\sqrt{2}) \sum_i \left[g_i^{(L)*} a_{Li} + g_i^{(R)*} a_{Ri} \right], \end{aligned} \quad (\text{A4})$$

$$\begin{aligned} \dot{a}_2 &= i(g + \Delta)a_2 + i\chi a_1 b^\dagger + \Omega/\sqrt{2} \\ &\quad - (i/\sqrt{2}) \sum_i \left[g_i^{(L)*} a_{Li} - g_i^{(R)*} a_{Ri} \right], \end{aligned} \quad (\text{A5})$$

$$\dot{b} = -i\omega_m b + i\chi a_2^\dagger a_1 - i \sum_i g_{bi}^* b_i, \quad (\text{A6})$$

$$\dot{a}_{Li} = -i(\omega_{Li} - \omega_d) a_{Li} - i g_i^{(L)} (a_1 + a_2) / \sqrt{2}, \quad (\text{A7})$$

$$\dot{a}_{Ri} = -i(\omega_{Ri} - \omega_d) a_{Ri} - i g_i^{(R)} (a_1 - a_2) / \sqrt{2}. \quad (\text{A8})$$

Under the Markovian approximation, we introduce the decay rates γ_L , γ_R , and γ_m of the optical modes in the left and right cavities, the mechanical mode as well as the corresponding fluctuation operators [31], then we can obtain the dynamical equation of the cavity modes and the mechanical modes in Eqs. (2)-(4) by noting that $\gamma_L = \gamma_R = \gamma_c$. The equations of motion of J_- , J_z , and b are obtained in Eqs. (18)-(20). With the condition $\gamma_c \gg \gamma_m$, by eliminating the operator of the cavity modes with adiabatic approximation, we can obtain the equations of motion of the phonon given in Eq. (21), with the corresponding fluctuation operator defined as

$$\begin{aligned} \Gamma(t) &= \alpha \left[\Gamma_2^\dagger(t) a_1 + a_2^\dagger \Gamma_1(t) \right] \\ &\quad - \frac{i\alpha\chi}{\sqrt{2}} \left[\frac{\Omega\Gamma_1^\dagger(t)}{N + i\gamma_c\Delta} - \frac{\Omega^*\Gamma_2(t)}{N - i\gamma_c\Delta} \right] b \\ &\quad + \frac{\alpha \left[\frac{\gamma_c}{2} - i(g - \Delta) \right] \Omega\Gamma_2^\dagger(t)}{\sqrt{2} [N + i\gamma_c\Delta]} + \sqrt{2\gamma_m} b_{in}(t). \end{aligned} \quad (\text{A9})$$

Appendix B: Parameters given in subsection IV B

By adiabatically eliminating the cavity variables, the phonon inversion operator J_z can be written as

$$J_z \approx \frac{\Sigma_z(\Delta, \delta)}{(|\varepsilon_1|^2 + 4\chi^2 b^\dagger b)(N^2 + \gamma_c^2 \Delta^2)}. \quad (\text{B1})$$

where the term $\Sigma_z(\Delta, \delta)$ is defined as

$$\begin{aligned} \Sigma_z &= g|\Omega|^2 \Delta |\varepsilon_1|^2 + 2\chi^2 \delta \Delta |\Omega|^2 b^\dagger b \\ &\quad - i\chi |\varepsilon_1|^2 |\Omega|^2 (b^\dagger N - N b) / (2\gamma_c) \\ &\quad + \chi |\Omega|^2 \{ i\varepsilon_1 [(N + \Delta^2)/2 + igM/\gamma_c] b + \text{h.c.} \}. \end{aligned} \quad (\text{B2})$$

We have defined $\varepsilon_1 = \gamma_c + i\delta$. In the regime near threshold, $n \ll |\varepsilon_1|^2 / (4\chi^2)$, up to the third-order terms J_z can be expanded as follow

$$J_z = j_0 + j_1 b + j_1^* b^\dagger - j_2 b^\dagger b + j_3 b^\dagger b^\dagger b + j_3^* b^\dagger b b, \quad (\text{B3})$$

with $j_0 = g\Delta|\Omega|^2\varepsilon_3$ and other coefficients j_i (with $i = 1, 2, 3$)

$$j_1 = i\chi\varepsilon_3|\Omega|^2 [M + (\varepsilon_2 M + \gamma_c \varepsilon_1 \Delta^2) / |\varepsilon_1|^2] / (2\gamma_c), \quad (\text{B4})$$

$$j_2 = 2\chi^2 \Delta \varepsilon_3 |\Omega|^2 [\omega_m / |\varepsilon_1|^2 + gM\varepsilon_3], \quad (\text{B5})$$

$$\begin{aligned} j_3 &= [i\chi^3 \varepsilon_3 |\Omega|^2 / (2\gamma_c |\varepsilon_1|^2)] \\ &\quad \times [(2\varepsilon_3 M^2 - 1) |\varepsilon_1|^2 + 2\varepsilon_3 (\varepsilon_2^* M^2 + \gamma_c \varepsilon_1^* \Delta^2 M) \\ &\quad - \varepsilon_2^* + 4M + 4(\varepsilon_2^* M + \gamma_c \varepsilon_1^* \Delta^2) / |\varepsilon_1|^2]. \end{aligned} \quad (\text{B6})$$

where the parameters $M = \gamma_c^2 / 4 + g^2$, $\varepsilon_2 = \gamma_c^2 - 2g\delta + 2ig\gamma_c + i\gamma_c\delta$, and $\varepsilon_3 = 1 / (M^2 + \gamma_c^2 \Delta^2)$.

Substituting J_z in Eq. (B3) into the dynamical equation of b in Eq. (23), if we define coefficients G_i (for $i = 0, 1, \dots, 4$)

$$G_0 = \eta_1 + i\eta_2, \quad (\text{B7})$$

$$G_1 = \eta_3 - \gamma_m - i(\omega_m + \eta_4), \quad (\text{B8})$$

$$G_2 = 2\chi^2 j_1^* / \varepsilon_1 + \eta_5 + i\eta_6, \quad (\text{B9})$$

$$G_3 = 2\chi^2 j_1 / \varepsilon_1, \quad (\text{B10})$$

$$G_4 = \eta_7 - i\eta_8, \quad (\text{B11})$$

then phonon lasing equation near the threshold can be written as in Eq. (25) with the parameters

$$\eta_1 = \chi\gamma_c\varepsilon_3|\Omega|^2 (\varepsilon_4 M + 2\delta\Delta^2) / (2|\varepsilon_1|^2), \quad (\text{B12})$$

$$\eta_2 = \chi\varepsilon_3|\Omega|^2 (\varepsilon_5 M + 2\gamma_c^2 \Delta^2) / (2|\varepsilon_1|^2), \quad (\text{B13})$$

$$\eta_3 = \gamma_c\chi^2 (2j_0 - \delta\Delta|\Omega|^2\varepsilon_3) / |\varepsilon_1|^2, \quad (\text{B14})$$

$$\eta_4 = \chi^2 (2\delta j_0 + \gamma_c^2 \Delta |\Omega|^2 \varepsilon_3) / |\varepsilon_1|^2, \quad (\text{B15})$$

$$\begin{aligned} \eta_5 &= \gamma_c\chi^3 \varepsilon_3 |\Omega|^2 / (2|\varepsilon_1|^2) \\ &\quad \times [\varepsilon_4 - 2\varepsilon_3 M |\Omega|^2 (\varepsilon_4 M + 2\delta\Delta^2)], \end{aligned} \quad (\text{B16})$$

$$\begin{aligned} \eta_6 &= \chi^3 \varepsilon_3 |\Omega|^2 / (2|\varepsilon_1|^2) \\ &\quad \times [\varepsilon_5 - 2\varepsilon_3 M |\Omega|^2 (\varepsilon_5 M + 2\gamma_c^2 \Delta^2)], \end{aligned} \quad (\text{B17})$$

$$\eta_7 = 2\gamma_c\chi^2 (j_2 - 2\delta\chi^2 \Delta \varepsilon_3^2 |\Omega|^2 M) / |\varepsilon_1|^2, \quad (\text{B18})$$

$$\eta_8 = 2\chi^2 (\delta j_2 + \chi^2 \gamma_c^2 \Delta \varepsilon_3^2 |\Omega|^2 M) / |\varepsilon_1|^2. \quad (\text{B19})$$

Here we have defined $\varepsilon_4 = \delta + 2g$ and $\varepsilon_5 = \gamma_c^2 - 2\delta g$.

Using the semi-classical approximation, the phonon field b can be written as a two-dimensional vector, $b = (u_1, u_2)^T$. Thus, we can obtain the dynamical equations for u_1 and u_2 as

$$\begin{aligned} \dot{u}_1 &= \eta_1 + \alpha' u_1 - \text{Im}(G_1) u_2 + (\eta_5 + \varepsilon_6) u_1^2 + \varepsilon_7 u_1 u_2 \\ &\quad + (\eta_5 - \delta\varepsilon_8/\gamma_c) u_2^2 - (u_1^2 + u_2^2) (\eta_7 u_1 + \eta_8 u_2) \end{aligned} \quad (\text{B20})$$

$$\begin{aligned} \dot{u}_2 &= \eta_2 + \alpha' u_2 + \text{Im}(G_1) u_1 + (\eta_6 - \varepsilon_8) u_2^2 + \varepsilon_9 u_1 u_2 \\ &\quad + (\eta_6 - \delta\varepsilon_6/\gamma_c) u_1^2 - (u_1^2 + u_2^2) (\eta_7 u_2 - \eta_8 u_1) \end{aligned} \quad (\text{B21})$$

with the corresponding coefficients

$$\varepsilon_6 = 4\chi^2 \gamma_c \text{Re}(j_1) / |\varepsilon_1|^2, \quad (\text{B22})$$

$$\varepsilon_7 = 4\chi^2 [\delta \text{Re}(j_1) - \gamma_c \text{Im}(j_1)] / |\varepsilon_1|^2, \quad (\text{B23})$$

$$\varepsilon_8 = 4\chi^2 \gamma_c \text{Im}(j_1) / |\varepsilon_1|^2, \quad (\text{B24})$$

$$\varepsilon_9 = 4\chi^2 [\gamma_c \text{Re}(j_1) + \delta \text{Im}(j_1)] / |\varepsilon_1|^2. \quad (\text{B25})$$

In the special case of $\delta = 0$, then the conditions $\varepsilon_6 \gg \varepsilon_8, \eta_5, \eta_6$, and also $\eta_7 \gg \eta_8$, the dynamical equations of u_1

and u_2 can be written as

$$u_1 = \eta_1 + \alpha' u_1 - \text{Im}(G_1)u_2 + \varepsilon_6 u_1^2 - \varepsilon_8 u_1 u_2 + \eta_5 u_2^2 + \eta_8(u_1^2 + u_2^2)u_1 - \eta_8(u_1^2 + u_2^2)u_2. \quad (\text{B26})$$

$$u_2 = \eta_2 + \text{Im}(G_1)u_1 + \alpha' u_2 + \varepsilon_6 u_1 u_2 + (\eta_6 - \varepsilon_8)u_2^2 + \eta_6 u_1^2 + \eta_8(u_1^2 + u_2^2)u_2 + \eta_8(u_1^2 + u_2^2)u_1. \quad (\text{B27})$$

The conditions $\varepsilon_7 = -\varepsilon_8$ and $\varepsilon_9 = \varepsilon_6$ (for $\delta = 0$) have been used to obtain these equations.

Appendix C: Derivation for the dynamical equations for the fluctuation operators

Under the small fluctuation approximation as shown in Eqs. (13)-(15) and from Eqs. (2)-(4), we can write down the dynamical equations for the fluctuation operators as

$$\dot{\Lambda}_1(t) = -[\gamma_c/2 + i(g - \Delta)]\Lambda_1(t) + \Gamma_1(t) + i\chi[A_2\beta(t) + B_0\Lambda_2(t)], \quad (\text{C1})$$

$$\dot{\Lambda}_2(t) = -[\gamma_c/2 - i(g + \Delta)]\Lambda_2(t) + \Gamma_2(t) + i\chi[A_1\beta^\dagger(t) + B_0^*\Lambda_1(t)], \quad (\text{C2})$$

$$\dot{\beta}(t) = -(\gamma_m + i\omega_m)\beta(t) + \sqrt{2\gamma_m}b_{\text{in}}(t) + i\chi[A_2^*\Lambda_1(t) + A_1\Lambda_2^\dagger(t)]. \quad (\text{C3})$$

If we introduce the Fourier transform $f(t) = \int_{-\infty}^{+\infty} f(\omega) \exp(-i\omega t)(d\omega/2\pi)$ for arbitrary smooth function $f(t)$, the motion equations for the fluctuation operators in the frequency domain can be written as

$$-i\omega\tilde{\Lambda}_1(\omega) = -[\gamma_c/2 + i(g - \Delta)]\tilde{\Lambda}_1(\omega) + \tilde{\Gamma}_1(\omega) + i\chi[A_2\tilde{\beta}(\omega) + B_0\tilde{\Lambda}_2(\omega)], \quad (\text{C4})$$

$$-i\omega\tilde{\Lambda}_2(\omega) = -[\gamma_c/2 - i(g + \Delta)]\tilde{\Lambda}_2(\omega) + \tilde{\Gamma}_2(\omega) + i\chi[A_1\tilde{\beta}^\dagger(\omega) + B_0^*\tilde{\Lambda}_1(\omega)], \quad (\text{C5})$$

$$-i\omega\tilde{\beta}(\omega) = -(\gamma_m + i\omega_m)\tilde{\beta}(\omega) + \sqrt{2\gamma_m}\tilde{b}_{\text{in}}(\omega) + i\chi[A_2^*\tilde{\Lambda}_1(\omega) + A_1\tilde{\Lambda}_2^\dagger(\omega)]. \quad (\text{C6})$$

By eliminating the fluctuation operators $\tilde{\Lambda}_1(\omega)$ and $\tilde{\Lambda}_2(\omega)$,

we can obtain the expression of $\tilde{\beta}(\omega)$ in Eq. (30). The corresponding coefficients p_i ($i = 1, 2, \dots, 6$) are given by

$$p_1 = \left(\sqrt{2\gamma_m}\lambda_1 - \chi^2 A_2^* B_0 n_2\right) / D_1, \quad (\text{C7})$$

$$p_2 = i\chi(A_1 n_2^+ \lambda_1 + i\chi A_2^* B_0 n_1 m_2) / D_1, \quad (\text{C8})$$

$$p_3 = i\chi[A_1 n_3^+ \lambda_1 + A_2^* + i\chi A_2^* B_0(n_4 + n_1 m_3)] / D_1, \quad (\text{C9})$$

$$p_4 = i\chi[A_1 n_4^+ \lambda_1 + i\chi A_2^* B_0(n_3 + n_1 m_4)] / D_1, \quad (\text{C10})$$

$$p_5 = i\chi[A_1 n_5^+ \lambda_1 + i\chi A_2^* B_0(n_6 + n_1 m_5)] / D_1, \quad (\text{C11})$$

$$p_6 = i\chi[A_1 n_6^+ \lambda_1 + i\chi A_2^* B_0(n_5 + n_1 m_6)] / D_1, \quad (\text{C12})$$

and the corresponding coefficients $\lambda_i(\omega)$ ($i = 1, 2, \dots, 4$), $m_i(\omega)$ ($i = 1, 2, \dots, 6$), and $n_i(\omega)$ ($i = 1, 2, \dots, 6$) are defined as

$$\lambda_1 = \gamma_c/2 + i(g - \Delta) - i\omega, \quad (\text{C13})$$

$$\lambda_2 = \gamma_c/2 - i(g + \Delta) - i\omega, \quad (\text{C14})$$

$$\lambda_3 = \gamma_m + i\omega_m - i\omega, \quad (\text{C15})$$

$$\lambda_4 = \lambda_1 \lambda_2 + \chi^2 |B_0|^2, \quad (\text{C16})$$

$$m_1 = i\chi^3 A_1^* A_2 B_0^* (\lambda_4 + \lambda_4^+) / (D_2 \lambda_3^+ \lambda_4 \lambda_4^+), \quad (\text{C17})$$

$$m_2 = \sqrt{2\gamma_m} / (\lambda_3^+ D_2), \quad (\text{C18})$$

$$m_3 = \chi^2 A_1^* B_0^* / (\lambda_3^+ \lambda_4 D_2), \quad (\text{C19})$$

$$m_4 = i\chi A_2 (\chi^2 |B_0|^2 - \lambda_4^+) / (\lambda_1^+ \lambda_3^+ \lambda_4^+ D_2), \quad (\text{C20})$$

$$m_5 = -i\chi \lambda_1 A_1^* / (\lambda_3^+ \lambda_4 D_2), \quad (\text{C21})$$

$$m_6 = -\chi^2 A_2 B_0^* / (D_2 \lambda_3^+ \lambda_4^+), \quad (\text{C22})$$

$$n_1 = i\chi(A_1 \lambda_1 + i\chi B_0^* A_2 m_1^+) / \lambda_4, \quad (\text{C23})$$

$$n_2 = -\chi^2 B_0^* A_2 m_2^+ / \lambda_4, \quad (\text{C24})$$

$$n_3 = -\chi^2 B_0^* A_2 m_3^+ / \lambda_4, \quad (\text{C25})$$

$$n_4 = i\chi(B_0^* + i\chi B_0^* A_2 m_4^+) / \lambda_4, \quad (\text{C26})$$

$$n_5 = -\chi^2 B_0^* A_2 m_5^+ / \lambda_4, \quad (\text{C27})$$

$$n_6 = (\lambda_1 - \chi^2 B_0^* A_2 m_6^+) / \lambda_4. \quad (\text{C28})$$

with

$$D_1 = \lambda_1 \lambda_3 - i\chi A_1 n_1^+ \lambda_1 + \chi^2 A_2^* B_0 n_1 m_1 + \chi^2 |A_2|^2, \quad (\text{C29})$$

and $D_2 = 1 + \chi^2 |A_2|^2 / (\lambda_1^+ \lambda_3^+) - \chi^2 |A_1|^2 \lambda_1 / (\lambda_3^+ \lambda_4) - \chi^4 |B_0|^2 |A_2|^2 / (\lambda_1^+ \lambda_3^+ \lambda_4^+)$.

-
- [1] D. Leibfried, R. Blatt, C. Monroe, and D. Wineland, *Rev. Mod. Phys.* **75**, 281 (2003).
[2] N. W. Ashcroft and N. D. Mermin, *Solid State Physics* (Saunders College Publishing, New York, 1976).
[3] M. Poot and H. S. J. van der Zant, *Phys. Rep.* **511**, 273 (2012).
[4] X. Hu and F. Nori, *Phys. Rev. Lett.* **76**, 2294 (1996); *ibid.* **79**, 4605 (1997).
[5] W. A. Kütt, W. Albrecht and H. Kurz, *IEEE J. Quantum Electron.* **28**, 2434 (1992).
[6] E. B. Tucker, *Phys. Rev. Lett.* **6**, 547 (1961).
[7] W. E. Bron and W. Grill, *Phys. Rev. Lett.* **40**, 1459 (1978).
[8] A. J. Kent, R. N. Kini, N. M. Stanton, M. Henini, B. A. Glavin, V. A. Kochelap, and T. L. Linnik, *Phys. Rev. Lett.* **96**, 215504 (2006).
[9] G. Bahl, M. Tomes, F. Marquardt, and T. Carmon, *Nat. Phys.* **8**, 203 (2012).
[10] A. D. O'Connell, M. Hofheinz, M. Ansmann, R. C. Bialczak, M. Lenander, E. Lucero, M. Neeley, D. Sank, H. Wang, M. Weides, J. Wenner, J. M. Martinis, and A. N. Cleland, *Nature (London)* **464**, 697 (2010).
[11] M. D. LaHaye, J. Suh, P. M. Echternach, K. C. Schwab, and M. L. Roukes, *Nature (London)* **459**, 960 (2009).

- [12] T. Rocheleau, T. Ndikum, C. Macklin, J. B. Hertzberg, A. A. Clerk, and K. C. Schwab, *Nature (London)* **463**, 72 (2010).
- [13] T. J. Kippenberg and K. J. Vahala, *Science* **321**, 1172 (2008).
- [14] I. Mahboob, K. Nishiguchi, H. Okamoto, and H. Yamaguchi, *Nat. Phys.* **8**, 387 (2012).
- [15] X. W. Xu, H. Wang, J. Zhang, and Y. X. Liu, *Phys. Rev. A* **88**, 063819 (2013).
- [16] X. W. Xu, Y. J. Zhao, and Y. X. Liu, *Phys. Rev. A* **88**, 022325 (2013).
- [17] J. Q. Liao, H. K. Cheung, and C. K. Law, *Phys. Rev. A* **85**, 025803 (2012).
- [18] J. Q. Liao and F. Nori, *Phys. Rev. A* **88**, 023853 (2013).
- [19] J. Kabuss, A. Carmele, T. Brandes, and A. Knorr, *Phys. Rev. Lett.* **109**, 054301 (2012).
- [20] J. T. Mendonca, H. Tercas, G. Brodin, and M. Marklund, *Euro-Phys. Lett.* **91**, 33001 (2010).
- [21] E. M. Chudnovsky and D. A. Garanin, *Phys. Rev. Lett.* **93**, 257205 (2004).
- [22] P. A. Fokker, J. I. Dijkhuis, and H. W. de Wijn, *Phys. Rev. B* **55**, 2925 (1997).
- [23] I. Camps and S. S. Makler, *Solid State Commun.* **116**, 191 (2000).
- [24] I. Bargatin and M. L. Roukes, *Phys. Rev. Lett.* **91**, 138302 (2003).
- [25] K. Vahala, M. Hermann, S. Knünz, V. Batteiger, G. Saathoff, T. W. Hänsch, and T. Udem, *Nat. Phys.* **5**, 682 (2009).
- [26] I. Mahboob, K. Nishiguchi, A. Fujiwara and H. Yamaguchi, *Phys. Rev. Lett.* **110**, 127202 (2013).
- [27] R. P. Beardsley, A. V. Akimov, M. Henini, and A. J. Kent, *Phys. Rev. Lett.* **104**, 085501 (2010).
- [28] J. B. Khurgin, M. W. Pruessner, T. H. Stievater, and W. S. Rabinovich, *Phys. Rev. Lett.* **108**, 223904 (2012).
- [29] J. B. Khurgin, M. W. Pruessner, T. H. Stievater, and W. S. Rabinovich, *New J. Phys.* **14**, 105022 (2012).
- [30] I. S. Grudin, H. Lee, O. Painter, and K. J. Vahala, *Phys. Rev. Lett.* **104**, 083901 (2010).
- [31] M. O. Scully and M. S. Zubairy, *Quantum Optics* (Cambridge University Press, Cambridge, England, 1997).
- [32] Z. R. Gong, H. Ian, Y. X. Liu, C. P. Sun, and F. Nori, *Phys. Rev. A* **80**, 065801 (2009).
- [33] H. Miao, S. Danilishin, T. Corbitt, and Y. Chen, *Phys. Rev. Lett.* **103**, 100402 (2009).
- [34] S. Basiri-Esfahani, U. Akram, and G. J. Milburn, *New J. Phys.* **14**, 085017 (2012).
- [35] G. Heinrich and F. Marquardt, *Europhys. Lett.* **93**, 18003 (2011).
- [36] M. Ludwig, A. H. Safavi-Naeini, O. Painter, and F. Marquardt, *Phys. Rev. Lett.* **109**, 063601 (2012).
- [37] P. Kóár, S. D. Bennett, K. Stannigel, S. J. M. Habraken, P. Rabl, P. Zoller, and M. D. Lukin, *Phys. Rev. A* **87**, 013839 (2013).
- [38] X. W. Xu and Y. J. Li, *J Phys. B* **46**, 035502 (2013).
- [39] F. Massel, S. U. Cho, J. M. Pirkkalainen, P. J. Hakonen, T. T. Heikkilä, and M. A. Sillanpää, *Nat. Commun.* **3**, 987 (2012).
- [40] M. Zhang, G. S. Wiederhecker, S. Manipatruni, A. Barnard, P. McEuen, and M. Lipson, *Phys. Rev. Lett.* **109**, 233906 (2012).
- [41] C. A. Regal, J. D. Teufel, and K. W. Lehnert, *Nat. Phys.* **4**, 555 (2008).
- [42] J. D. Thompson, B. M. Zwickl, A. M. Jayich, F. Marquardt, S. M. Girvin, and J. G. E. Harris, *Nature (London)* **452**, 72 (2008).
- [43] S. Aldana, C. Bruder, and A. Nunnenkamp, *Phys. Rev. A* **88**, 043826 (2013).
- [44] O. Kyriienko, T. C. H. Liew, and I. A. Shelykh, *Phys. Rev. Lett.* **112**, 076402 (2014).
- [45] J. J. Sakurai, *Modern Quantum Mechanics* (Addison Wesley Publishing, New York, 1994).
- [46] H. Haken, *Light, Vol. II, Laser Light Dynamics* (North-Holland Physics Publishing, Amsterdam, 1985).
- [47] K. Børkje, A. Nunnenkamp, and S. M. Girvin, *Phys. Rev. Lett.* **107**, 123601 (2011).
- [48] B. Peng, S. K. Ozdemir, F. Lei, F. Monifi, M. Gianfreda, G. L. Long, S. Fan, F. Nori, C. M. Bender, and L. Yang, *Nat. Phys.* **10**, 394 (2014).
- [49] H. Jing, S. K. Ozdemir, X.-Y. Lu, J. Zhang, L. Yang, and F. Nori, arXiv:1403.0657 (2014).
- [50] X.-W. Xu, Y.-X. Liu, C.-P. Sun, and Y. Li, arXiv:1402.7222 (2014).